Available online at www.sciencedirect.com
ScienceDirect
Journal of Power Sources 179 (2008) 863–869
JOURNAL OF POWER SOURCES
www.elsevier.com/locate/jpowsour

Correlation of electrical and physical properties of photoanode with hydrogen evolution in enzymatic photo-electrochemical cell

Sanghyun Bae [a], Junwon Kang [a], Eunjung Shim [b], Jaekyung Yoon [c], Hyunku Joo [c,*]

[a] *Department of Environmental Engineering, Yonsei University, 234 Maeji-ri, Hungub-myun, Wonju, Gangwon-do 220-710, Republic of Korea*
[b] *Department of Chemistry, Chungnam National University, 220 Gung-dong, Yuseong-gu, Daejeon 305-764, Republic of Korea*
[c] *Fossil Energy & Environment Research Department, Korea Institute of Energy Research, 71-2 Jang-dong, Yuseong-gu, Daejeon 305-343, Republic of Korea*

Received 3 September 2007; accepted 19 December 2007
Available online 17 January 2008

Abstract

In this study, the electrical and physical properties, including the current density, open-circuit voltage, morphology and crystalline structure, of an anodized TiO_2 electrode on a titanium foil are correlated with the hydrogen production rate in an enzymatic photo-electrochemical system. The effect of light intensity at ca. 74 and ca. 146 mW cm^{-2} on the properties is also examined. Anodizing (20 V; bath temperature 5 °C; anodizing time 45 min) and subsequent annealing (350–850 °C for 5 h) of the Ti foils in an O_2 atmosphere led to the formation of a tube-shaped, or a compact layered, TiO_2 film on the Ti substrate depending on the annealing temperature. The annealing temperature has a similar effect on the properties of the sample and the hydrogen evolution rate. The generated electrical value, the chronoamperometry (CA), is +13 to −229 and +13 to −247 μA for light intensities of ca. 74 and ca. 146 mW cm^{-2}, while the corresponding open-circuit voltage (OCV) is in the range of −41 to −687 and −144 to 738 mV, respectively. In the absence of light (dark), the CA is 13–29 μA and the OCV is +258 to −126 mW cm^{-2}. The trend in the electrical properties for the different samples is well matched with the rate of hydrogen evolution. The samples with higher activities (450, 550, and 650 °C) have similar X-ray diffraction (XRD) patterns, which clearly indicates that the samples showing the highest evolution rate are composed of both anatase and rutile, while those showing a lower evolution rate are made of either anatase or rutile. Increasing the intensity of the irradiated light causes a remarkable enhancement in the rate of hydrogen production from 71 to 153 μmol h^{-1} cm^{-2}.

Keywords: Hydrogen evolution; Photoanode; Anodization; Immobilized; Enzymatic photo-electrochemical cell

1. Introduction

There is growing interest in hydrogen which has the potential to supplement and ultimately replace fossil fuels for the production of energy. Moreover, the emission of greenhouse gases also needs to be reduced to help solve the problem of climate change. The light-driven electrolysis of water using a semiconductor photoanode is a non-polluting, wasteless, renewable method of energy production, because water can be split into hydrogen and oxygen. In order to raise the efficiency of the photo-electrochemical conversion (PEC) of solar energy, it is essential to design a cell configuration that is energetically coordinated, stably operated, and economically feasible. This conclusion is derived from the fact that the efficiency of the photo-electrochemical production of hydrogen is determined by a combination of factors, such as imperfections in the crystalline structure, bulk and surface properties of the semiconductor photoanode, its resistance to corrosion in electrolytes, and its ability to drive the water-splitting reaction [1]. Following the pioneering work of Fujishima and Honda [2], a huge number of publications have been produced in the field of the photo-electrochemical production of hydrogen [3,4].

The photocatalytic process has, however, been simultaneously criticized as being uneconomical compared with other oxidative treatment systems and modern hydrogen production systems, due to its inherently low efficiency and the limitations resulting from the necessity for novel materials, an appropriate light source, and immobilization, which may increase the overall energy costs [5]. Therefore, in contrast to other research groups, our attention has focused on developing enzymatic photocatalytic systems. Comprehensive reviews have been published on semiconductor particulate systems [5], TiO_2 photocatalysts [6]

* Corresponding author. Tel.: +82 42 860 3563; fax: +82 42 860 3134.
E-mail address: hkjoo@kier.re.kr (H. Joo).

0378-7753/$ – see front matter © 2008 Elsevier B.V. All rights reserved.
doi:10.1016/j.jpowsour.2007.12.117

and other material-related issues [3,7] pertaining to hydrogen production. Compared with other photocatalysts, TiO_2 is much more promising, as it is stable, non-corrosive, environmentally friendly, abundant and cost-effective [6]. Recently, photoanodes covered with TiO_2-based films have been investigated using techniques such as anodization [8–13] and sputtering [14]. A nanotube-film on titanium foil produced by anodization has attracted our particular interest as a stable, light-sensitizing photoanode for the enzymatic production of hydrogen driven by light.

A previous study [15] proposed a different approach using a light-sensitized enzymatic (LSE) system. The LSE system is a way of producing hydrogen by coupling an inorganic semiconductor with enzymes in a photo-electrochemical configuration. The system uses the intrinsic proton reduction ability of hydrogenase enzyme in tandem with an anodic compartment in which electron donors, such as water, undergo oxidative reaction on a light-sensitized photoanode. The generated electrons are separated and moved to the cathodic compartment through an external circuit and used to reduce protons into hydrogen on the active sites of the enzymes. In this study, the oxidized ions move to the cathodic compartment through an ion bridge such as a nanofiltration (NF) membrane and, at the same time, a solar cell applies an external bias. The proposed LSE system replaces the in vitro biological system used for hydrogen production in which complex electron transport systems, known as main barriers, exist such as the photosystems (PS) II and I, and ferredoxin (FD). These electron transport systems can conceivably be replaced with a photocatalyst or photoanode. Thus, the photocatalyst sensitized by light irradiation produces electrons and holes (electron vacancies), which can then be separated to reduce the protons and oxidize the electron donor.

The present work aims to establish a method of characterizing the LSE system, by correlating the physical and electrical properties of the anodized TiO_2 electrode with the trend in hydrogen evolution in the LSE system.

2. Experimental

2.1. Sample preparation

All chemicals were used without further purification. P25 TiO_2 (Degussa, FRG) served as a reference for the methylene blue (MB, 95% Showa chemical, Japan) which was used as the probe compound for measuring the photocatalytic activity of the anodized TiO_2 electrode (ATE). Titanium foils (0.25 mm thick, 99.6% purity, Goodfellow, England) were cut into pieces (2 cm × 2 cm) for anodization. The anodization was performed at 20 V for 45 min at 5 °C with magnetic agitation in 0.5 vol.% hydrofluoric (HF) acid, after which the samples were annealed in an oxygen atmosphere (400 ml min^{-1}) at 350–850 °C for 5 h. A detailed explanation about the role of each component of the anodizing solution is available in the literatures [10,13].

The illuminated area of the working electrode (photoanode) was 1 cm^2. An electrical contact was made on the backside of the titanium foil after scribing out the oxide layer. Then, an electrically insulated copper wire was attached to the backside using silver paste and non-conductive epoxy resin. A 0.05 M Tris–HCl buffer was also prepared and used as a cathodic electrolyte (Trizma base, minimum 99.9% titration and 2N HCl, Sigma). Purified hydrogenase (*Pyrococcus furiosus*, '*Pfu*' hereafter) was purchased from Prof. Adams at the University of Georgia. The activity assay of *Pfu* (21,834 unit ml^{-1}) was much higher than that of *Clostridium butyricum* (1442 unit ml^{-1}) and *Thiocapsa roseopersicina* (1704 unit ml^{-1}), as determined with Tris–HCl (50 mM, pH 8.5, 50 °C, absorbance at 570 nm). The specific activity (unit mg^{-1}, Bio-rad protein assay, absorbance at 750 nm) of *Pfu* was two-to-three times higher than that of the latter hydrogenases. One unit of hydrogenase activity catalyzes the production of 1 μmol of H_2 min^{-1}. Methyl viologen (MV) from Sigma was used as an electron relay.

2.2. Apparatus and analysis

The experiments were mainly conducted in a two-compartment (anodic and cathodic elements connected via a NF membrane and a solar cell panel) reactor, as shown in Fig. 1. The cylindrical-shaped anodic compartment had a volume of 80 ml (headspace volume ca. 55 ml) and contained an aqueous solution of 1.0 M KOH for water oxidation unless otherwise noted. The cathodic compartment was a water-jacketed, cylindrical-shaped cell (80 ml, headspace volume ca. 55 ml) with Tris–HCl buffer sealed with a silicone rubber gasket. Prior to the reaction, the mixture was de-aerated with argon gas for 30 min to remove the oxygen in the water and headspace. Two terminals from a solar cell panel (10 cm × 10 cm, crystalline silicon, max. 1.5 V) were attached to the ATE and the platinum mesh cathode, respectively, in order to apply an external bias to the system. An NF membrane (molecular weight cut-off, MWCO = 200) made of polyamide (SU-210, Toray, Japan) was inserted between the

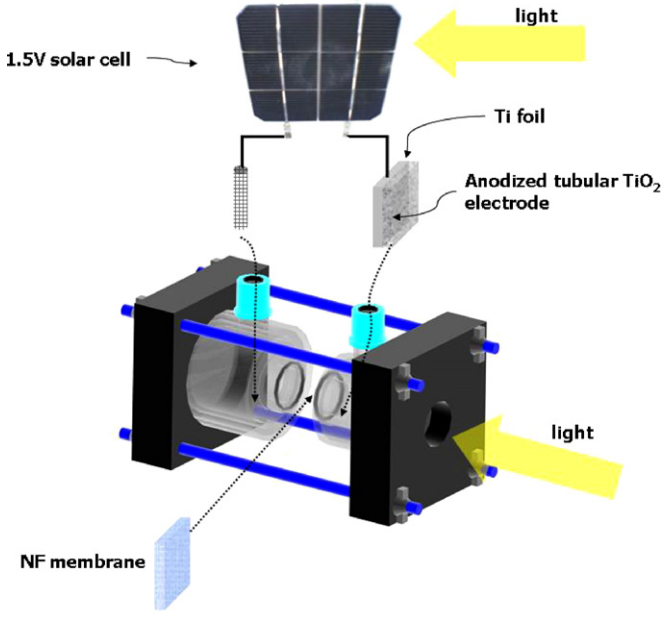

Fig. 1. Schematic view of reactor with anodized tubular TiO_2 photoanode, solar cell, and NF membrane for hydrogen production.

two cells to permit ion transport, while preventing the transport of the enzyme and MV.

Chronoamperometry (CA), cyclic voltammetry (CV), and open-circuit voltage (OCV) measurements were performed when necessary with a potentiostat (G300 w/PHE200 software, GAMRY Instruments Electrochemistry, PA, USA) with a platinum mesh electrode as a counter electrode (CE) and Ag|AgCl (saturated in 3.0 M KCl) as a reference electrode (RE). The light source was a 1000 W xenon lamp (Oriel, USA), which was filtered through a 10-cm IR water filter. The irradiated light intensity was ca. 74 ± 3.4–146 ± 2.3 mW cm^{-2} (at 360 ± 50 nm), but the light intensity absorbed by the sample seemed to be slightly lower than the irradiated intensity, due to the loss by reflection and absorption at the reactor window and electrolyte. The crystal phase and size were determined by X-ray diffraction (XRD, Miniflex, Rigaku; $k = 0.89$, $\lambda = 0.15418$ for Cu Kα X-ray, 30 kV, 15 mA) and the change in absorbance of the MB was measured with UV–vis spectroscopy (SCINCO, S-3150, Korea). The structure and morphology were investigated using scanning electron microscopy (SEM/EDAX, Hitachi S-4700) and field emission transmission electron microscopy (FE-TEM, Tecnai F30 S-Twin, FEI, Netherlands). The hydrogen and oxygen produced were analyzed by a gas chromatograph with a thermal conductivity detector (TCD at 260 °C, oven at 40 °C). The col-

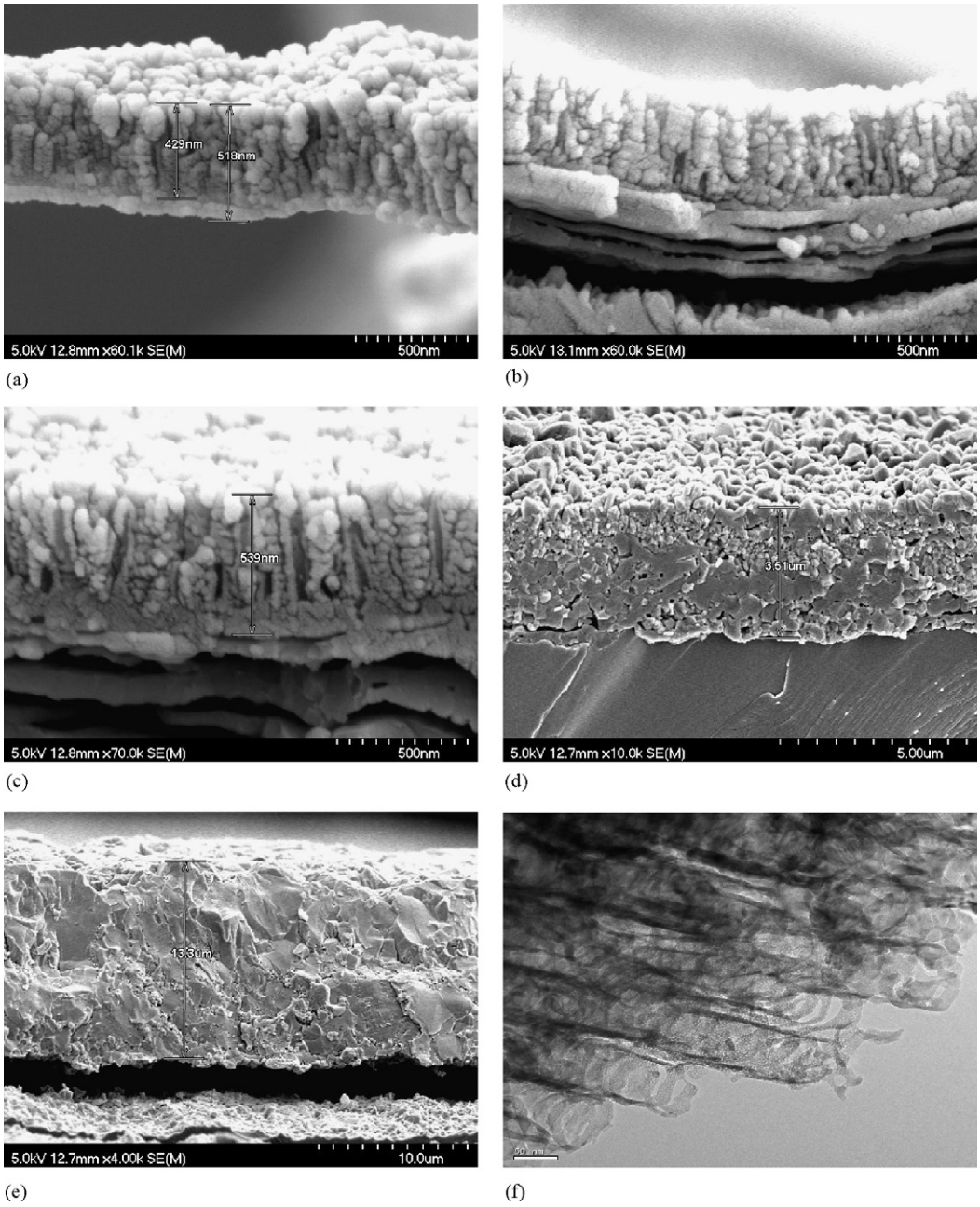

Fig. 2. SEM images of selected anodized tubular TiO_2 electrodes with different annealing temperatures for 5 h (side view, anodization at 20 V/45 min and 5 °C in 0.5 vol.% HF) and HR-TEM of tubes peeled off from anodized tubular TiO_2 electrodes (550 °). (a) 450 °C; (b) 550 °C; (c) 650 °C; (d) 750 °C; (e) 850 °C and (f) HR-TEM (550 °C).

umn used in the system was a molecular sieve 5A (Supelco, USA).

3. Results and discussion

The SEM images of selected samples anodized in 0.5 vol.% HF are shown in Fig. 2. A clean TiO_2 tube was evident only in the sample anodized at the bath temperature of 25 °C (Fig. 2(f)), while the ones anodized at 5 °C (Fig. 2(a)–(e)) were comprised of a continuous nanoporous layer and a compact oxide layer of even height. Increasing the annealing temperature produces a highly dense film with a thickness of 13.3 μm. The morphology of the porous film is known to be affected by the electrolyte, electrolyte concentration, electrolyte pH, anodizing time and temperature, and the annealing ambient conditions. This is because porous structures are formed during the anodization through two processes: field-enhanced oxidation and field-enhanced oxide dissolution. Furthermore, solid-state sintering is likely to take place at elevated temperature, which leads to grain growth, densification, and ultimately the complete collapse of the structure. These changes are more remarkable during the phase transformations which often accompany bond-breaking and enhanced mass transport [8,9]. The HR-TEM image of tubes peeled off from the sample (anodized at 20 V in 0.5 vol.% HF at 5 °C, then heat-treated in O_2 at 550 °C for 5 h, Fig. 2(f)) clearly presents a lateral view of the nanotubes with a wall thickness of ca. 14.5 nm and periodic ring structure, as well as a crystal fringe at the wall.

All of the as-deposited samples are found to be amorphous, while heat-treatment in dry O_2 ambient supported the formation of anatase phase up to 650 °C and rutile phase from 475 °C when the samples are initially anodized in 0.5 vol.% HF (Fig. 3(a)). In the absence of any equilibrium phase transformation temperature, no stable rutile phases are produced at the low annealing temperature, heating rate or duration time used for the preparation of the sample. In the diffraction patterns, complete transformation to rutile phase occurs at a temperature close to 750 °C. Of particular note is that the similar half-width of the anatase peak between 350 and 650 °C and the increasing half-width of the rutile peak in the investigated range demonstrate that the growth of anatase crystals is restricted by the constraints imposed by the walls, while the irreversible transformation to stable rutile phase increases at elevated temperatures and the coalescence of the rutile crystals form larger crystallites [9]. The peak height does not increase linearly with the anodization time (Fig. 3(b)). On the other hand, the temperature of the anodization bath, pH and anodizing voltage are all known to affect the wall thickness, length and inner diameter of the tubes [8,9].

The photocatalytic activity of the ATE was first checked by monitoring the MB discolouration rate ($[MB]_o = 10\,mg\,L^{-1}$ in 200 mL solution, 200 mg of P25 or 2 cm × 2 cm ATE). Unlike P25, the samples give a lower MB discoloration rate, irrespective of the preparation conditions. A lower dose of P25 (10, 5, 2 mg of P25), however, shows similar profiles to the ATE samples. Langmuir-Hinshelwood kinetics, generally applied in photocatalysis, indicate that a relatively high concentration of a probe material converts the equation to zero-order kinetics. This is indicated in our study by varying the amount of P25 with a

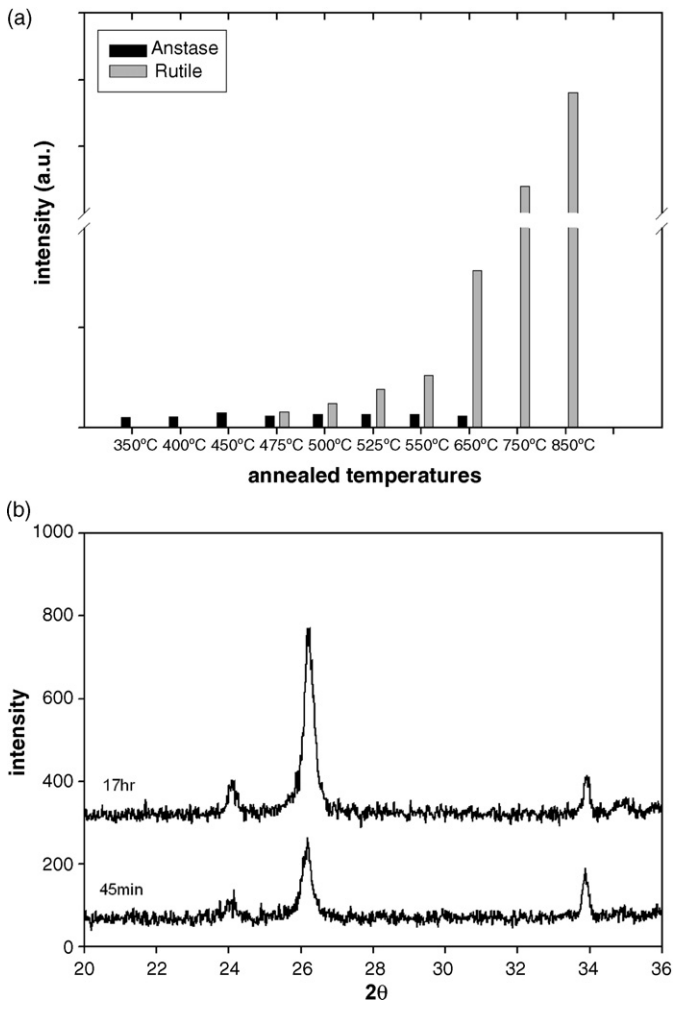

Fig. 3. (a) XRD peak intensities of crystalline of selected TiO_2 electrodes and (b) effect of anodization time on crystallinity (anodization at 20 V and 5 °C in 0.5 vol.% HF).

fixed initial MB concentration ($10\,mg\,L^{-1}$), in order to change the time-coursed profiles of MB discolouration from first-order to zero-order kinetics with decreasing injection amount. The amount of TiO_2 on the Ti substrate (2 cm × 2 cm) is calculated to be 2.3 ± 0.7 mg, assuming a film thickness in the range of 1.5 μm and a TiO_2 density of $3.9\,g\,cm^{-3}$. This amount is about one-tenth that of P25 (200 mg initially), which is well correlated with the fact that less than 5 mg of P25 shows a similar discolouration rate to the prepared samples.

Enzymatic hydrogen evolution in the anodic compartment with oxygen in the cathodic compartment was performed with an external bias (ca. 1.5 V) applied by a solar cell. Prior to the reactions, chronoamperometry, open-circuit voltage and cyclic voltammetry (in the range of −1.5 to +1.5 V) measurements were performed with a potentiostat to facilitate the understanding of the physical meaning of the obtained values. The working electrode (WE) was placed on either the photoanode (P25 on ITO substrate) or the Pt cathode, while the CE was on the other together with the RE, which comprised Ag|AgCl in saturated KCl. An external bias ranging from −1.5 to +1.5 V was then applied to the WE through the potentiostat.

The application of either a positive bias to the photoanode or a negative bias to the Pt cathode generates a negative or positive current, indicating that the electrons flow from the photoanode to the cathode in both cases. This upward shift of the anodic energy level led to hydrogen evolution in the cathode compartment.

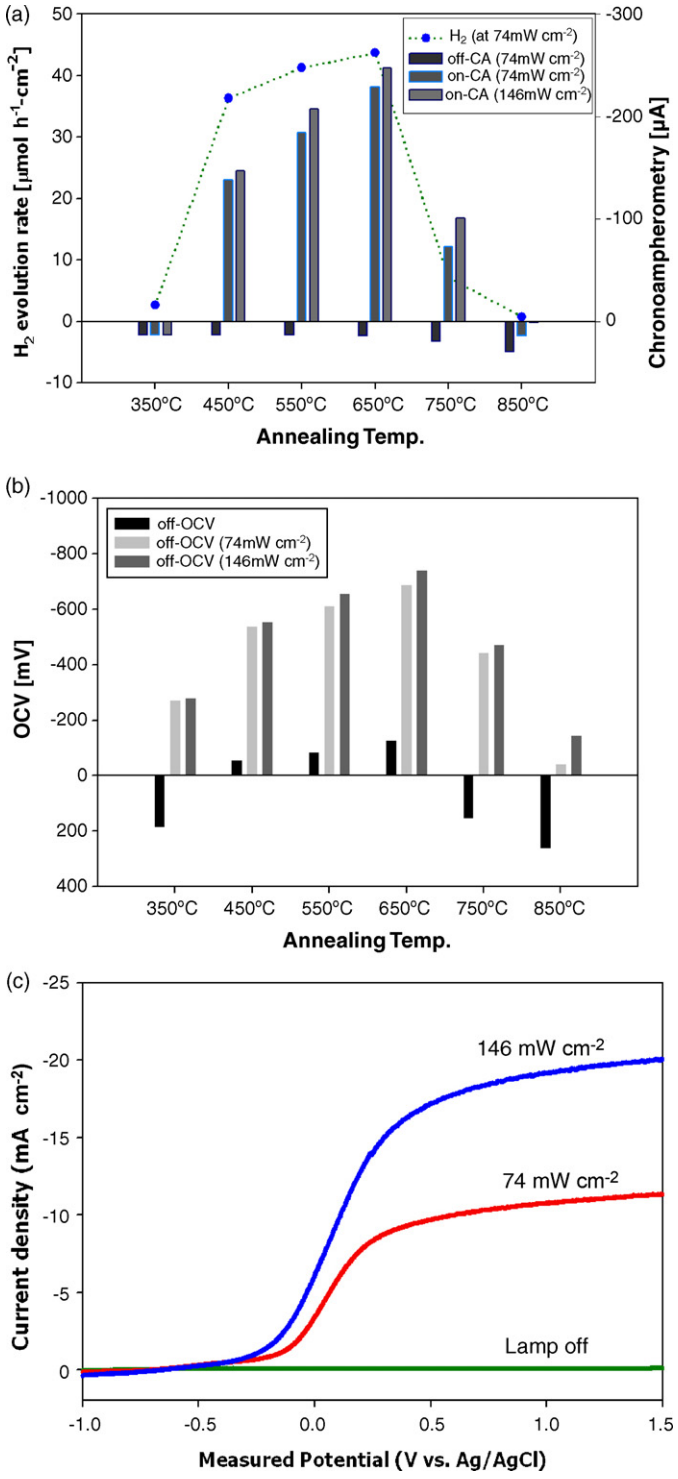

Fig. 4. Correlation between hydrogen evolution rate and electrical properties: (a) H_2 evolution rate (at 74 mW cm^{-2} for 2 h) and chronoampherometry; (b) open-curcuit voltage with the samples; (c) cyclic voltammetry (sample annealed at 650 °C).

The generated electrical values are a CA in the range of +13 to −229 μA at a light intensity of ca. 74 mW cm^{-2} and in the range of +13 to −247 μA at light intensity of ca. 146 mW cm^{-2} (Fig. 4(a)), while the OCV is in the range of −41 to −687 mV at a light intensity of ca. 74 mW cm^{-2} and −144 to 738 mV at a light intensity of ca. 146 mW cm^{-2} (Fig. 4(b)). In the absence of light irradiation (dark), the CA is 13–29 μA and the OCV is +258 to −126 mW cm^{-2}, which clearly demonstrates the effect of light (Fig. 4(a) and (b)).

Cyclic voltammetry was used to investigate the effect of light and its intensity on the current density with samples annealed at 650 °C (Fig. 4(c)), in terms of the photocurrent and dark-current response for the sample. The ATE showed n-type behaviour, i.e., a positive photocurrent at anodic potentials [16].

After the aforementioned electrochemical values were obtained, a solar cell and a photoanode were both irradiated to increase the Fermi level and excite electrons from the valence band (VB) into the conduction band (CB) of the photoanode. With the *Pfu* amount optimized at 10.98 units, this system configuration led to the stoichiometric evolution of H_2 and O_2 (H_2:O_2 = ca. 2:1). Noticeably, the trend of hydrogen evolution with the samples coincided well with the CA and OCV values measured during the light irradiation, as shown in Fig. 4(a). The samples annealed at temperatures between 450 and 650 °C have higher values than the other samples, probably due to the crystal isomorphs evident in Fig. 3(a), as these samples consist of some proportion of both anatase and rutile. Easy electron transport from the light-sensitized oxide layers to the substrates through the interface region may be essential in the system. Without any KOH, ATE and *Pfu*, the system shows much lower activity in terms of the H_2 and O_2 evolution. Prolonging the reaction time to 3 h with different light intensities leads to an increase in the evolution rate from 41 to 71 μmol cm^{-2} h^{-1} for 74 mW cm^{-2} and from 82 to 153 μmol cm^{-2} h^{-1} for 146 mW cm^{-2}. This indicates that the system requires 1 h of lag time before it is stabilized (Fig. 5). Doubling the light intensity clearly produces more hydrogen, but further increase in light intensity does not yield a linear increase in the amount of hydrogen evolved, which is to be expected because it is known that the reaction rate is

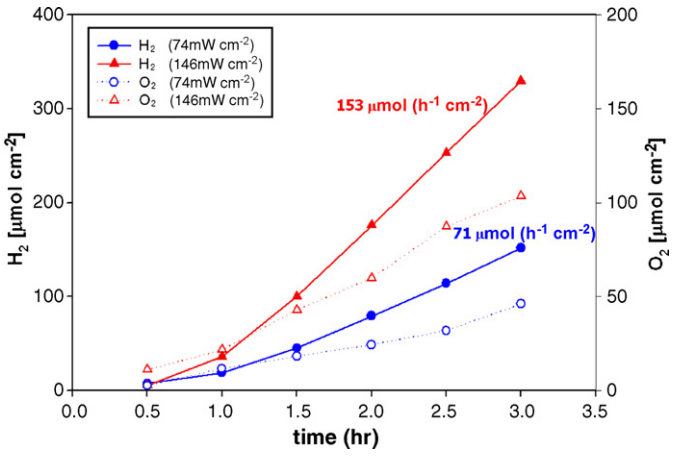

Fig. 5. Time-coursed profile of hydrogen and oxygen evolution on ATE under different light intensities (20 V/45 min and 650 °C/5 h in 0.5 vol.% HF).

proportional to the light intensity only up to a certain threshold above which the rate of point charge recombination dominates the reaction rate [17]. In general, a first-order reaction rate with respect to light intensity means that the system is not saturated with respect to the light intensity [18].

A schematic representation with energy diagrams of the system used in this study is shown in Fig. 6. Without light irradiation, charge transfer occurs at the surface of an immersed semiconductor and band bending occurs because of the difference in the electron affinity or electrochemical potential of the two phases (Fig. 6(a)). If the semiconductor photoanode absorbs light, electrons move towards the bulk, while holes move towards the surface and are injected into the electrolyte. Hence, the band bending is reduced and the Fermi level shifts upward. At this time, the energy level of water oxidation (O_2/H_2O) should be above the valence band (VB) of the photoanode and that of the proton reduction (H^+/H_2) should be below the Fermi level of the metal cathode (Fig. 6(b)) to split water. When an additional external bias is applied, a further shift of the Fermi level is obtained and the ability of the electrons to reduce protons is also increased (Fig. 6(c)).

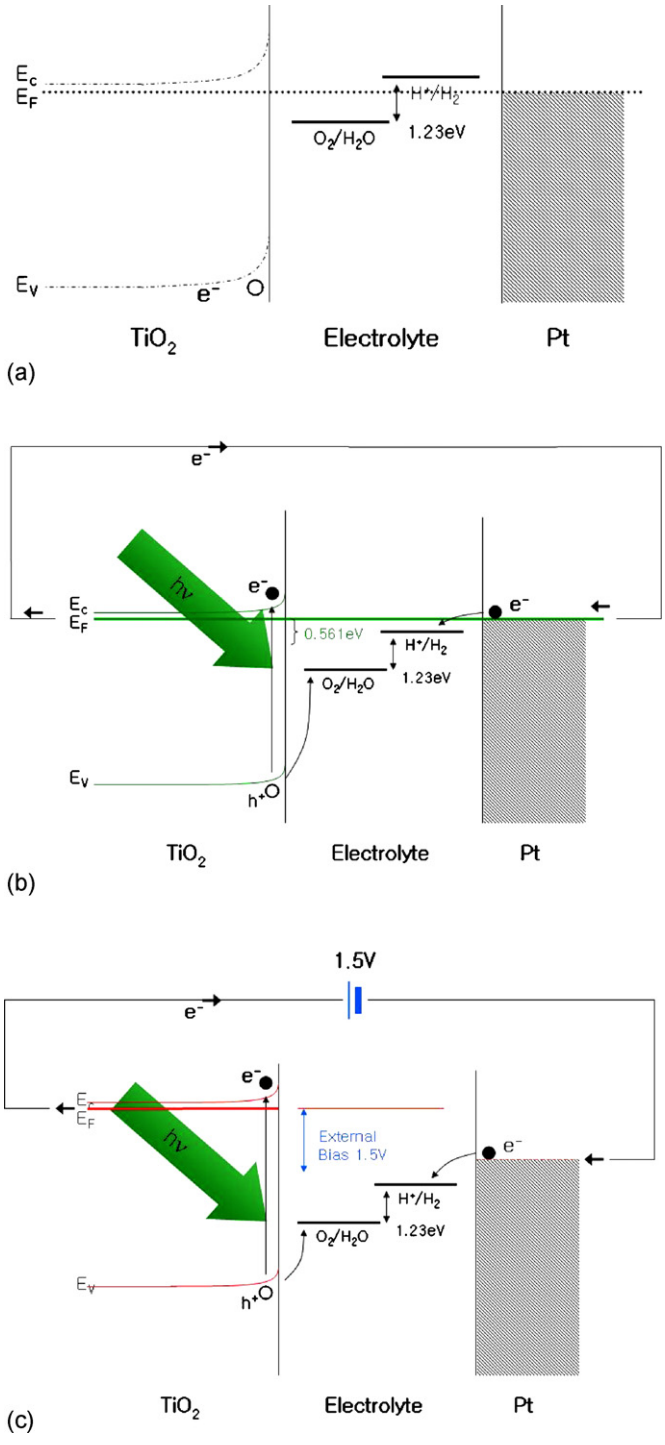

Fig. 6. Schematic representation with energy diagrams of the used system: (a) without light irradiation; (b) with light irradiation; (c) with light and solar cell applied.

The rate of hydrogen production was ca. 71 μmol h^{-1} cm^{-2}, i.e., ca. 15.7 L h^{-1} m^{-2}. A rough calculation suggests that on a fine sunny day with 6.5 h of sunlight, 1 023 750 L of H_2 could be evolved over an area of 10^4 m^2 (100 m × 100 m). Assuming that a fuel cell vehicle requires 4.6 kg of H_2 to travel 395 km, the evolved amount of H_2 is sufficient to charge ten vehicles for a journey of 7821 km.

The solar-to-hydrogen (STH) efficiency is approximately calculated according to:

$$\phi = \frac{K_{H_2}}{K_{irr}} \quad (1)$$

where K_{H_2} denotes the amount of H_2 produced in μmol cm^{-2} h^{-1} and K_{irr} the irradiated light in μmol photons cm^{-2} h^{-1}. According to Ref. [19], the UV intensity in solar irradiation is 1.5×10^{-6} mol s^{-1} per 1.4245×10^{-2} m^2, which equates to 37.8 μmol photon cm^{-2} h^{-1}. A total solar light intensity of 950–1375 μmol photon cm^{-2} h^{-1} could be obtained at AM 1.5 illumination. Therefore, the amount of hydrogen evolved, 71 μmol cm^{-2} h^{-1}, could be equivalent to an STH efficiency of ca. 6.1%.

4. Conclusions

For future hydrogen production with solar irradiation, a relatively novel approach has been introduced wherein a sensitized photoanode, prepared by anodization, donates electrons to hydrogenase through an external circuit that in turn reduces protons to hydrogen. To characterize the system more efficiently, the electrical and physical properties of the photoanode in the photoelectrochemical cell are correlated with the rate of hydrogen production. The trend of the electrical properties for the different samples is well matched with the rate of hydrogen evolution. Samples with higher activities have both anatase and rutile crystallines, while those with lower activities have either anatase or rutile. The simple measurement of the electrical properties of the photoanodes, prepared by various methods under different conditions, can be used to determine the amount of hydrogen that the photoanode is capable of producing. In this way, the number of time-consuming operations can be reduced and thereby assists the search for an optimized photoanode. This indirect characterization can be further utilized when the efficiency of the photoanode needs to be enhanced and controlled.

Acknowledgements

The research was performed for the Hydrogen Energy R&D Center, one of the 21st Century Frontier R&D Programs, funded by the Ministry of Science and Technology of Korea.

References

[1] V.M. Aroutiounian, V.M. Arakelyan, G.E. Shahnazaryan, Solar Energy 78 (5) (2005) 581–592.
[2] A. Fujishima, K. Honda, Nature 238 (1972) 37–38.
[3] T. Bak, J. Nowotny, M. Rekas, C.C. Sorrell, Int. J. Hydrogen Energy 27 (2002) 991–1022.
[4] S. Malato, J. Blanco, A. Vidal, C. Richter, Appl. Catal. B 37 (2002) 1–15.
[5] M. Ashokkumar, Int. J. Hydrogen Energy 23 (1998) 427.
[6] M. Ni, M.K.H. Leung, D.Y.C. Leung, K. Sumathy, Renew. Sust. Energy Rev. 11 (2007) 401.
[7] T. Bak, J. Nowotny, M. Rekas, C.C. Sorrell, Int. J. Hydrogen Energy 27 (2002) 19.
[8] D. Gong, C.A. Grimes, O.K. Varghese, W. Hu, R.S. Singh, Z. Chen, E.C. Dickey, J. Mater. Res. 16 (2001) 3331.
[9] O.K. Varghese, D. Gong, M. Paulose, C.A. Grimes, E.C. Dickey, J. Mater. Res. 18 (2003) 156.
[10] G.K. Mor, O.K. Vargheese, M. Paulose, N. Mukherjee, C.A. Grimes, J. Mater. Res. 18 (2003) 2588.
[11] G.K. Mor, K. Shankar, M. Paulose, O.K. Vargheese, C.A. Grimes, Nanoletters 5 (2005) 191.
[12] M. Paulose, G.K. Mor, O.K. Vargheese, K. Shankar, C.A. Grimes, J. Photochem. Photobiol. A: Chem. 178 (2006) 8.
[13] K.S. Raja, V.K. Mahajan, M. Misra, J. Power Sources 159 (2006) 1258.
[14] M. Kitano, M. Takeuchi, M. Matsuoka, J.M. Thomas, M. Anpo, Catal. Today 120 (2007) 133.
[15] J. Yoon, H. Joo, J. Korean, Chem. Eng. 24 (5) (2007) 742–748.
[16] T. Lindgren, M. Larsson, S.-E. Lindquist, Solar Energy Mater. Solar Cells 73 (2002) 377–389.
[17] M.A. Aguado, M.A. Anderson, C.G. Hill, J. Mol. Catal. 89 (1994) 165.
[18] S. Yamazaki, H. Tsukamoto, K. Araki, T. Tanimura, I. Tejedor, M.A. Anderson, Appl. Catal. B: Environ. 33 (2001) 109–117.
[19] D. Ljubas, Energy 30 (2005) 1699.